https://doi.org/10.5194/egusphere-2025-6044
Preprint. Discussion started: 3 February 2026

A unified physically based recession model reveals contrasting functioning of monsoon and Mediterranean karst aquifers

Liangjie Zhao[1,2,3], Yang Yang[1,4], Stefano Fazi[2], Song Luan[1,3], Cheng Li[1,4], Ning Zhang[1,4], and Elisabetta Preziosi[2]

[1]Institute of Karst Geology, Chinese Academy of Geological Sciences/ Key Laboratory of Karst Dynamics, Ministry of Natural Resources & Guangxi Zhuang Autonomous Region/ International Research Centre on Karst under the Auspices of UNESCO,Guilin,541004,China
[2]Water Research Institute (IRSA), National Research Council of Italy (CNR),Roma,00015,Italy
[3]Karst Water Resources and Environment Academician Workstation of Guizhou Province,Zunyi,563000,China
[4]Pingguo Guangxi, Karst Ecosystem, National Observation and Research Station,Pingguo,531406,China

Correspondence: Liangjie Zhao (zhaoliangjie0@gmail.com) and Yang Yang (yangyang_a@mail.cgs.gov.cn)

Abstract. Karst aquifers supply drinking water to hundreds of millions of people but remain among the least understood freshwater systems because of their strongly heterogeneous conduit–matrix structure. Spring recession analysis is widely used to infer karst storage dynamics, yet most existing models either treat different parts of the hydrograph separately or rely on empirical formulations with limited physical interpretability. Here we derive a unified analytical model for karst spring recession by combining turbulent conduit flow, represented by a Forchheimer-type relationship, with linear drainage from a porous matrix. The resulting governing equation, $\mathrm{d}Q/\mathrm{d}t = -\alpha Q^n + \gamma e^{-\lambda t}$, simultaneously describes nonlinear conduit depletion and delayed conduit–matrix exchange. The parameters α, n, γ, and λ are can be related to aquifer properties, reflecting conduit drainage efficiency, flow nonlinearity, and the magnitude and timescale of matrix drainage. We apply the model to hourly discharge records (2013–2023) from climatically and geologically contrasting karst systems in monsoon-influenced southwest China and Mediterranean central Italy. Event-based calibration shows that the unified recession model reproduces complete recession limbs and consistently outperforms a classical dual-reservoir benchmark. Beyond goodness of fit, the inferred parameter patterns reveal systematic regional contrasts: Chinese spring exhibits higher nonlinear exponents ($n = 2$) and larger α, indicating strongly turbulent, conduit-dominated drainage with short memory, whereas Italian spring is characterised by $n = 1$ and negligible γ, consistent with large, slowly draining matrix storage. Using regional-average parameter sets without further calibration, the unified recession model also reproduces independent multi-week drought recessions in both regions, demonstrating that these parameter contrasts are robust and transferable within each hydrogeological setting. Mapping events in the $(n, \tilde{S})$ parameter space delineates distinct functional regimes of karst aquifers that can be related to differences in drought resilience and baseflow support. The unified recession model thus provides a diagnostic tool to infer karst aquifer functioning from discharge data alone, supporting water-resource assessment and climate-impact studies in data-scarce regions.

Keywords. Karst aquifers; Spring recession; Physically based modelling; Conduit–matrix exchange; Regional hydrological functioning; Drought resilience

https://doi.org/10.5194/egusphere-2025-6044
Preprint. Discussion started: 3 February 2026

1 Introduction

Karst aquifers supply nearly a quarter of the global population with drinking water yet rank among the most dynamic and vulnerable hydrological systems. Their dual-porosity structure,comprising fast-flowing conduits embedded within a slow-draining porous matrix,drives complex hydrograph responses, particularly following rainfall events (Hartmann et al., 2014; Giese et al., 2025). Karst spring hydrographs typically exhibit a rapid rise and peak, followed by a prolonged, nonlinear recession limb. Understanding this recession phase is critical for characterizing storage dynamics, predicting drought resilience, and managing groundwater resources (Fiorillo, 2014; Zhang et al., 2025).

Traditional models like Maillet's exponential decay law (1905) describe spring recession using a single linear reservoir assumption. However, observed karst systems frequently deviate from simple exponential behavior, especially during early to intermediate recession stages (Wittenberg, 1999). These deviations reflect turbulent conduit flow, matrix leakage, structural heterogeneity, and climatic influences (Fauzi et al., 2021; Şen, 2020; Chin et al., 2009). Recent advances emphasize both physical realism and empirical flexibility (Sivelle et al., 2025). Basha (2020) derived analytical solutions from simplified dual-flow models, capturing multiple recession regimes (e.g., linear, square-root, exponential). Schuler et al. (2020) calibrated semi-distributed pipe-network models with high-frequency discharge data, revealing temporal shifts from conduit- to matrix-dominated flow. Wittenberg (1999)'s nonlinear reservoir framework enables flexible fitting of complex hydrographs and classification of spring types by flow-component dominance (Michel et al., 2003; Gan and Luo, 2013).Enhanced data and modeling tools now support deeper karst hydrograph interpretation (Olarinoye et al., 2020). Examples include KarstID for recession-based classification (Cinkus et al., 2023), dynamic storage estimation via recession parameters (Abirifard et al., 2022), and assessments of aquifer memory (Fatoni et al., 2024). Automated recession extraction (Çallı and Hartmann, 2022) and ensemble-data assimilation (Pansa et al., 2023) further enable large-scale analysis and uncertainty quantification (Cerino Abdin et al., 2021).Hydrological controls have also been scrutinized, including climate-induced biases in recession parameters (Jachens et al., 2020), rainfall-event impacts on conduit responses (Chang et al., 2021), and matrix–conduit exchange coefficients (Shirafkan et al., 2023), with regional flow-duration controls also documented (Ghotbi et al., 2020). Storage variation metrics have quantified precipitation influence in karst systems (Dong et al., 2025; Elhanati et al., 2024).

Conceptual and physical modeling progress includes head-driven flow in sinkhole-fed springs (Li et al., 2016), effective porosity–based recession models (Xu et al., 2018), siphon-flow mechanisms for intermittent springs (Guo et al., 2023), and recharge estimation in fractured-karst systems (Teixeira et al., 2023; Bauer et al., 2003). Comparative recession techniques assess seasonal flow changes (Kale et al., 2024), while foundational work on nonlinear flow (Reimann and Hill, 2009; Chen et al., 2015) informs process understanding.Recession curve analysis increasingly supports resource management and climate adaptation, addressing data-scarce catchments (Sivelle and Jourde, 2021), artificial regulation (Çelik et al., 2024), spring characterization via time-series metrics (Geravand et al., 2022; Mujib et al., 2024), and catchment-state identification (Rusjan et al., 2023). Despite these advances, a critical gap persists: no unified model reproduces the fast initial decline, nonlinear mid-term decay, and long-tail behavior of karst recessions within a single framework. Current approaches either focus on isolated recession

https://doi.org/10.5194/egusphere-2025-6044
Preprint. Discussion started: 3 February 2026

stages or rely on segmented fitting, introducing subjective bias and obscuring parameter interpretation (Shirafkan et al., 2021). Many models also lack physical grounding or climatic generalizability (Klammler et al., 2024).

In this study we address three questions. (i) Can the entire recession limb of karst spring hydrographs, from the early turbulent drainage phase to the prolonged tail, be described within a single physically consistent framework that explicitly represents both conduit and matrix processes? (ii) To what extent do the parameters of such a unified model provide robust and interpretable indicators of aquifer functioning, allowing us to distinguish conduit-dominated, matrix-influenced and mixed karst systems? (iii) Can parameter patterns inferred from recession curves be related to regional climatic and geological settings, thereby providing insight into the drought resilience and baseflow support of karst aquifers?

To address these questions, we derive a unified recession model from first principles of turbulent conduit flow and head-driven conduit–matrix exchange and apply it to high-resolution spring discharge records from monsoon and Mediterranean karst systems. By comparing the resulting parameter distributions and their uncertainties across regions, we interpret systematic contrasts in how karst aquifers store and release water under different hydro-climatic conditions.

2 Unified recession model(URM)

2.1 Conceptualisation and assumptions of the conduit–matrix system

Karst aquifers are commonly conceptualized as dual-domain systems in which a high-permeability conduit network is hydraulically coupled to a lower-permeability porous matrix (Ford and Williams, 2007; Hartmann et al., 2014). The integrated recession of the spring hydrograph emerges from the dynamic coupling between conduit and matrix domains, driven by time-varying hydraulic gradients. Denoting hydraulic head by h, in a one-dimensional representation along a conduit segment of characteristic length L, a mean head gradient can be approximated as $J \approx \Delta h/L$, where Δh is the head difference between upstream and downstream control volumes (Bear, 1972). Matrix–conduit exchange is represented here as a lumped head-dependent flux driven by the head difference between domain-averaged matrix head $h_m(t)$ and conduit head $h_c(t)$ (Warren and Root, 1963). Figure 1 illustrates this framework: matrix drainage supplies the conduit through distributed exchange fluxes driven by $h_m - h_c$. The hydraulic heads in the matrix and conduit, $h_m(t)$ and $h_c(t)$, may change at different rates in time, collectively controlling the spring discharge $Q(t)$. Matrix flow is assumed to follow Darcy's law. Conduit flow during recession is represented using a quadratic head-loss relation (Darcy–Forchheimer form), $\mathrm{d}h_c/\mathrm{d}x = aQ + bQ^2$, where a and b lump viscous and turbulent losses, respectively(Whitaker, 1996). During post-recharge recession, hydraulic gradients typically remain directed toward the outlet, so matrix-to-conduit exchange is predominantly unidirectional. This conceptualization provides the basis for the unified recession model derived below.

Starting from a 1-D momentum balance for conduit flow and a linear exchange representation for the matrix contribution, we obtain a governing equation for spring discharge. Assuming spatially averaged gradients and slowly varying exchange, the conduit resistance can be represented by an effective power-law recession term, while matrix drainage acts as an exponentially

https://doi.org/10.5194/egusphere-2025-6044
Preprint. Discussion started: 3 February 2026

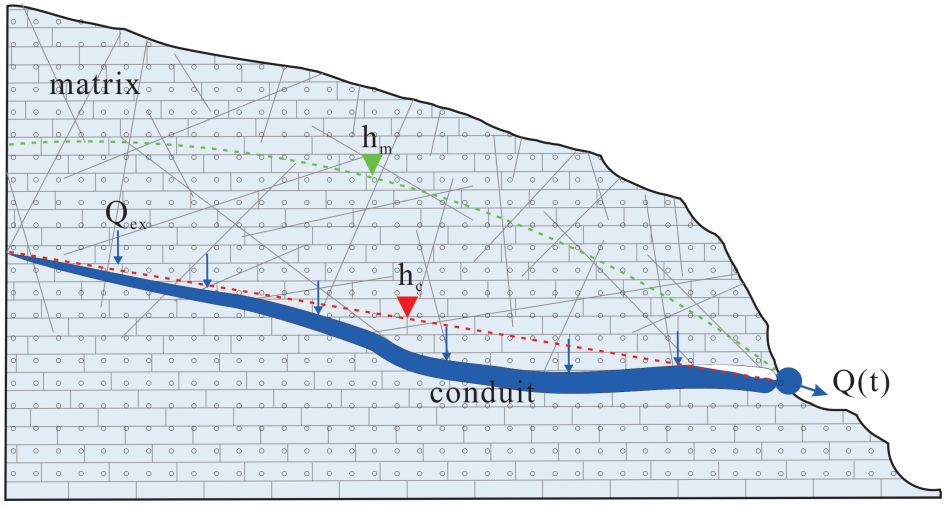

Figure 1. Conceptual model of coupled conduit–matrix flow during spring recession

decaying input. Under these approximations, the spring recession dynamics can be written as

$$\frac{\mathrm{d}Q}{\mathrm{d}t} = -\alpha Q^n + \gamma e^{-\lambda t} \tag{1}$$

We hereafter refer to equation (1) as the unified recession model (URM). where α and n capture the magnitude and nonlinearity of conduit drainage, respectively, and γ and λ describe the magnitude and decay rate of matrix-to-conduit exchange, respectively. For later interpretation we define the exchange-input scale $S \equiv \gamma/\lambda$, which equals the time integral of the exponentially decaying exchange term, $\int_0^\infty \gamma e^{-\lambda t}\,\mathrm{d}t = \gamma/\lambda$. Thus, S provides a compact measure of the potential magnitude of delayed matrix-to-conduit exchange contributing to the recession tail. We further use a parameter-space diagnostic by mapping events in the (n, S) space, where n is the drainage nonlinearity exponent. For regime classification we use the dimensionless ratio $\tilde{S} = S/Q_0$ (Sect. 4.3), where Q_0 is the discharge at the start of the recession segment.

Detailed steps of the asymptotic analysis and the identification of α, n, γ, and λ in terms of hydraulic and geometric properties are provided in Appendix A.

2.2 Relation to classical recession models

To evaluate the physical realism and generality of the unified recession model (URM; Eq. 1), Table 1 summarizes classical recession formulations and indicates how many of them can be recovered as special cases of the URM under specific parameter constraints or lumping assumptions. These include early empirical formulations (Boussinesq, 1904; Maillet, 1905; Coutagne, 1948), dual-component models (e.g., Mangin, 1975), nonlinear storage–discharge relationships (Wittenberg, 1999), and more recent physically based or data-driven approaches (e.g., Reimann et al., 2011; Rusjan et al., 2023). As shown in Table 1, many of these models represent special cases of the URM under specific parameter constraints. For instance: linear reservoir models with exponential decay (Maillet, 1905) correspond to the linear case $n = 1$; power-law recession models (Coutagne, 1948; Drogue, 1972) align with the nonlinear term αQ^n (with $\gamma = 0$); empirical long-tail or delayed-release components (Mangin,

https://doi.org/10.5194/egusphere-2025-6044
Preprint. Discussion started: 3 February 2026

Table 1. Summary of classical recession models and their correspondence to the unified recession model (URM)

Typical recession models	Mathematical form	Key assumptions	Recoverable from URM
Boussinesq (1904)	$Q(t) = Q_0/(1+\alpha' t)^2$	Dupuit assumption	$\gamma = 0,\ n = 1.5$
Maillet (1905)	$Q(t) = Q_0\, \mathrm{e}^{-\alpha t}$	Linear reservoir	$\gamma = 0,\ n = 1$
Coutagne (1948)	$Q(t) = Q_0\,[1+(n-1)\alpha t]^{\frac{n}{1-n}}$	Power-law storage	$\gamma = 0,\ n \neq 1$
Drogue (1972)	$Q(t) = Q_0/(1+\alpha' t)^m$	Gravity-driven drainage	$\gamma = 0,\ n = \frac{m+1}{m}$
Mangin (1975)	$Q(t) = Q_{r_0}\, \mathrm{e}^{-at} + q_0\, \frac{1+\eta t}{1+\epsilon t}$	Dual-reservoir system	$Q_{\text{fast}} + Q_{\text{slow}}$
Wittenberg (1999)	$\mathrm{d}Q/\mathrm{d}t = -k\,Q^b$	Single-reservoir	$\gamma = 0,\ n = b$
Barnes (1939) Schoeller (1948)	$Q(t) = \sum_{i=1}^{k} q_i\, \mathrm{e}^{-k_i t}$	Multi-reservoir	$\sum_i \gamma_i\, \mathrm{e}^{-\lambda_i t}$
Kirchner (2009)	diagnostic storage–discharge method	Multiple reservoirs and tailing term	$\gamma\, \mathrm{e}^{-\lambda t}$
Reimann et al. (2011)	CFP–MODFLOW (process model)	Turbulent in conduit, Darcy in matrix	URM-consistent
Li et al. (2016)	$Q(t) \propto (H_0 - H)^2$	Turbulent flow driven by head drop	URM-consistent
Basha (2020)	$Q(t) \propto \mathrm{e}^{-kt},\ t^{-1/2},\ t^{-1}$	Varying drainage phases	URM-consistent
Shirafkan et al. (2023)	$\mathrm{d}Q/\mathrm{d}t = f\big(Q(t), Q_{\text{ex}}\big)$	Matrix–conduit exchange control	URM-consistent
Rusjan et al. (2023)	$\mathrm{d}Q/\mathrm{d}t = g\big(Q(t), t, \text{state}\big)$	Data-driven dynamical system	URM-consistent

Note: "URM-consistent" indicates that the model is structurally compatible with Eq. (1) under lumping assumptions.

1975; Verhoest and Troch, 2000; Basha, 2020) can be represented, in the single-timescale limit, by the exponential term $\gamma \mathrm{e}^{-\lambda t}$. Even physically based exchange models (Reimann et al., 2011) and dynamical-systems formulations (Rusjan et al., 2023) show structural parallels to the unified equation. These correspondences confirm that the URM unifies diverse recession behaviors within a single framework while enhancing physical interpretability and modeling flexibility beyond purely empirical or fixed-structure approaches.

3 Data and Methods

3.1 Study Areas and Spring Data (China and Italy)

This study examines representative karst spring systems in both southern China and central Italy to evaluate the performance of the proposed recession model under contrasting geological and hydrological conditions. The Chinese study site is located in a region characterized by strong karst development, high conduit connectivity, and rapid drainage dynamics. In contrast, the Italian spring system represents a weakly karstified aquifer, with weaker structural permeability and slower recession behavior. The Zhaidi karst aquifer system is located in eastern Guilin City, Guangxi Province, China ($25°13'26.08''$–$25°18'58.04''$ N, $110°31'25.71''$–$110°37'30''$ E; Figure 2).The catchment drains an area of about 33 km^2 This synclinal valley exhibits a marked topographic contrast, with a central lowland area at approximately 198 m elevation bordered by ridges to the east and west reaching up to 900.1 m This pronounced relief generates a strong north–south hydraulic gradient that governs regional groundwater flow. The hydrogeological setting is predominantly composed of carbonate rocks,

https://doi.org/10.5194/egusphere-2025-6044
Preprint. Discussion started: 3 February 2026

which account for 83.9% of the catchment area. The stratigraphy includes highly karstified Upper Devonian pure limestones (D_3d), moderately permeable Middle Devonian dolomites (D_2t), non-karstic Upper Devonian sandstones (D_3x), and Quaternary alluvial deposits (Q) The G047 spring serves as a major discharge outlet for the aquifer, emerging along a NE–SW–oriented fault zone. Recharge is primarily allogenic, conveyed through the G037 sinkhole, which integrates surface runoff into a master conduit approximately $2175\ \mathrm{m}$ in length, with an average hydraulic gradient of $23.90‰$ The region is characterized by a humid subtropical monsoon climate, with a mean annual precipitation of $1613\ \mathrm{mm}$, approximately 78.00% of which occurs between May and September. This seasonal concentration of rainfall results in substantial variability in spring discharge, ranging from 0.10 to $25.30\ \mathrm{m^3\,s^{-1}}$, predominantly governed by rapid conduit flow responses to storm events.

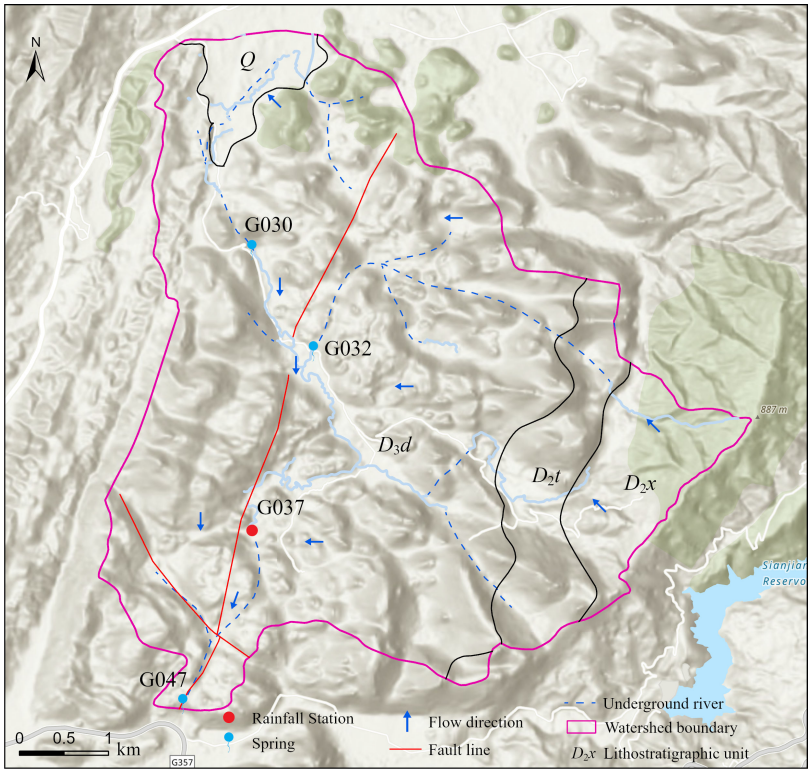

Figure 2. Geological and hydrological setting of the Zhaidi karst system in China (Basemap: World Topographic Map. Sources: Esri and its data providers | Powered by Esri).

Lupa Spring is located east of Arrone (Umbria, central Italy) along the right-bank footslope of the Fosso di Rosciano valley, at $365\ \mathrm{m}$ a.s.l. $(42°33′44.05″–42°36′17.80″\ \mathrm{N},\ 12°48′18.39″–12°53′36.29″\ \mathrm{E};$ Figure 3) The contributing catchment area is $18\ \mathrm{km^2}$ The subsurface divide is governed not only by topography but, more importantly, by several steeply dipping faults and associated damage zones. The principal aquifer is a fractured–karstic carbonate sequence locally mantled by a thin alluvial–colluvial veneer. The spring issues where the fault zone intersects the eroded valley flank and the bedrock–valley-fill contact is exposed, in correspondence with a box-fold anticline developed within a Mesozoic–Cenozoic limestone and marly-limestone sequence (Umbrian–Marche succession)(Preziosi et al., 2022). Recharge occurs on the surrounding carbonate hills

https://doi.org/10.5194/egusphere-2025-6044
Preprint. Discussion started: 3 February 2026

and groundwater migrates toward the valley through interconnected fractures and joints, with faults acting as preferential flow conduits. Discharge at Lupa Spring is sustained by the large storage and natural regulation capacity of the deep carbonate massif together with the structural control of the drainage pathways. Consequently, seasonal fluctuations are muted and the hydrograph is dominated by a persistently stable baseflow. Based on the daily precipitation record for the Lupa spring catchment (2013–2023), obtained from the publicly available hydrological database of Regione Umbria (Regione Umbria), mean annual precipitation is 1459 mm, with rainfall seasonally skewed toward autumn–winter and only 34 % occurring from May to September. Under these conditions, Lupa Spring exhibits a persistently stable baseflow, with discharge varying between 0.25 and $0.30\ \mathrm{m^3\,s^{-1}}$ throughout the year.

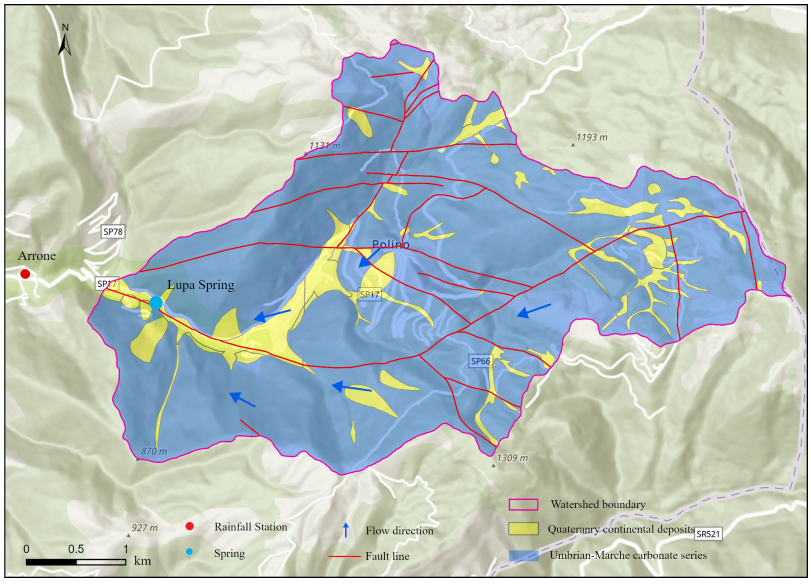

Figure 3. Geological and hydrological setting of the Lupa spring in Italy (Basemap: World Topographic Map. Sources: Esri and its data providers | Powered by Esri).

To ensure comparability across contrasting hydrogeological settings, we applied uniform criteria to select recession events for model calibration and validation. Each event had to satisfy the following conditions: (i) a minimum duration of 10 consecutive days (≥ 240 h) of uninterrupted recession in the absence of effective rainfall, defined as no precipitation events producing a measurable increase in spring discharge; (ii) for the Chinese springs, an initial discharge $> 10\ \mathrm{m^3\ s^{-1}}$ (Figure 4), consistent with the high transmissivity and large flow magnitudes characteristic of intensely karstified systems; and (iii) for the Italian springs, an initial discharge $> 0.20\ \mathrm{m^3\ s^{-1}}$ (Figure 5), reflecting the more moderate discharge behaviour of weakly karstified aquifers.

3.2 Parameter Estimation and Model Bencharmking

URM parameters $(\alpha, n, \gamma, \lambda)$ were estimated for individual recession events by nonlinear least squares, using a Levenberg–Marquardt algorithm with multiple random initialisations to reduce the risk of local minima. To benchmark the performance of the URM, we conducted a comparative analysis against the classical dual-reservoir model developed by Mangin (1975). The

https://doi.org/10.5194/egusphere-2025-6044
Preprint. Discussion started: 3 February 2026

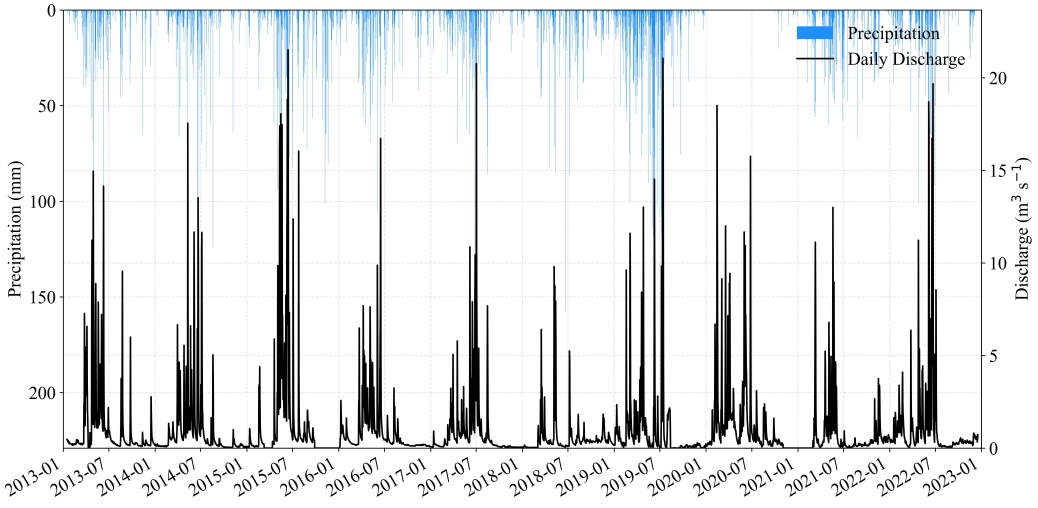

Figure 4. Time series of spring discharge and precipitation at Zhaidi for the period 2013–2023

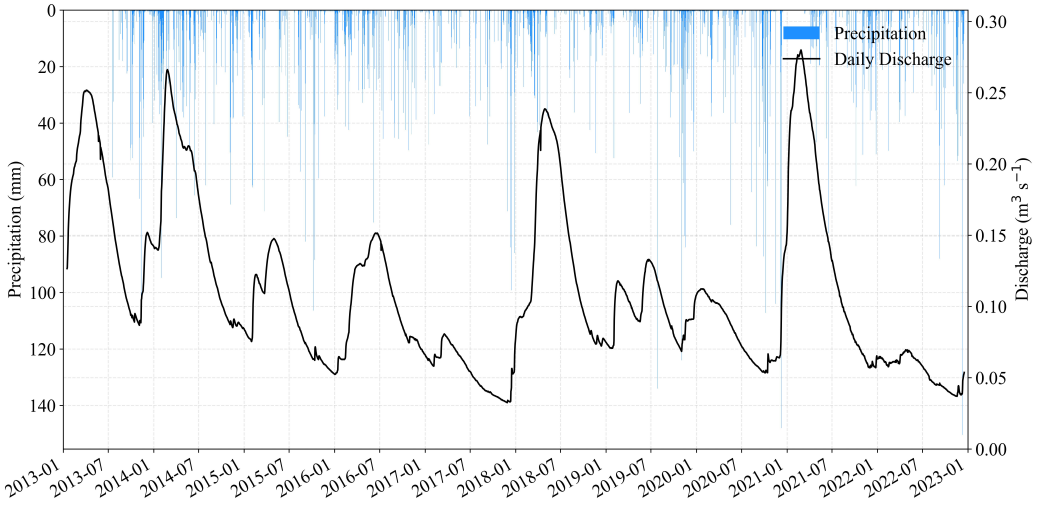

Figure 5. Time series of spring discharge and precipitation at Lupa for the period 2013–2023

155 Mangin's model describes spring recession as a superposition of fast and slow reservoir responses, expressed analytically as

$$Q(t) = q_{r0}\,\mathrm{e}^{-at} + q_0\,\frac{1+\eta t}{1+\epsilon t}$$

where q_{r0}, q_0, a, η, and ϵ are five calibration parameters. While Mangin's model is not a strict special case of URM, its structure is qualitatively comparable to the URM in that Eq. (1) combines a drainage term controlling the early-time decay (with the linear-reservoir case $n = 1$ as a limiting form) with a delayed-release term controlling the late-time tail, so the classical

https://doi.org/10.5194/egusphere-2025-6044
Preprint. Discussion started: 3 February 2026

dual-reservoir model provides a natural benchmark for comparison. Model performance was evaluated with the Kling–Gupta efficiency (KGE) and the root-mean-square error (RMSE) computed in discharge space.

4 Results and Discussion

4.1 Model Performance and Representative Recessions

Figure 6 presents observed recession curves alongside simulations from the URM and the Mangin benchmark model for all 12 events. Across the ten Chinese recession events depicted in Figure 6a–j (duration 189–427 h), the URM successfully reproduces the complete hydrograph without requiring subjective segmentation. The model achieves a median KGE of 0.945 (0.915–0.970) and a median RMSE of $0.36\ \mathrm{m^3\,s^{-1}}$ (0.26–0.40). Its performance is broadly comparable to the Mangin model, which attains a median KGE of 0.970 and RMSE of $0.305\ \mathrm{m^3\,s^{-1}}$. The fitted URM parameters consistently cluster around $n \approx 2$ and α values between 0.01 and 0.03, with non-zero γ and λ values essential for capturing the sustained baseflow. This parameter set is diagnostic of a conduit-dominated system.

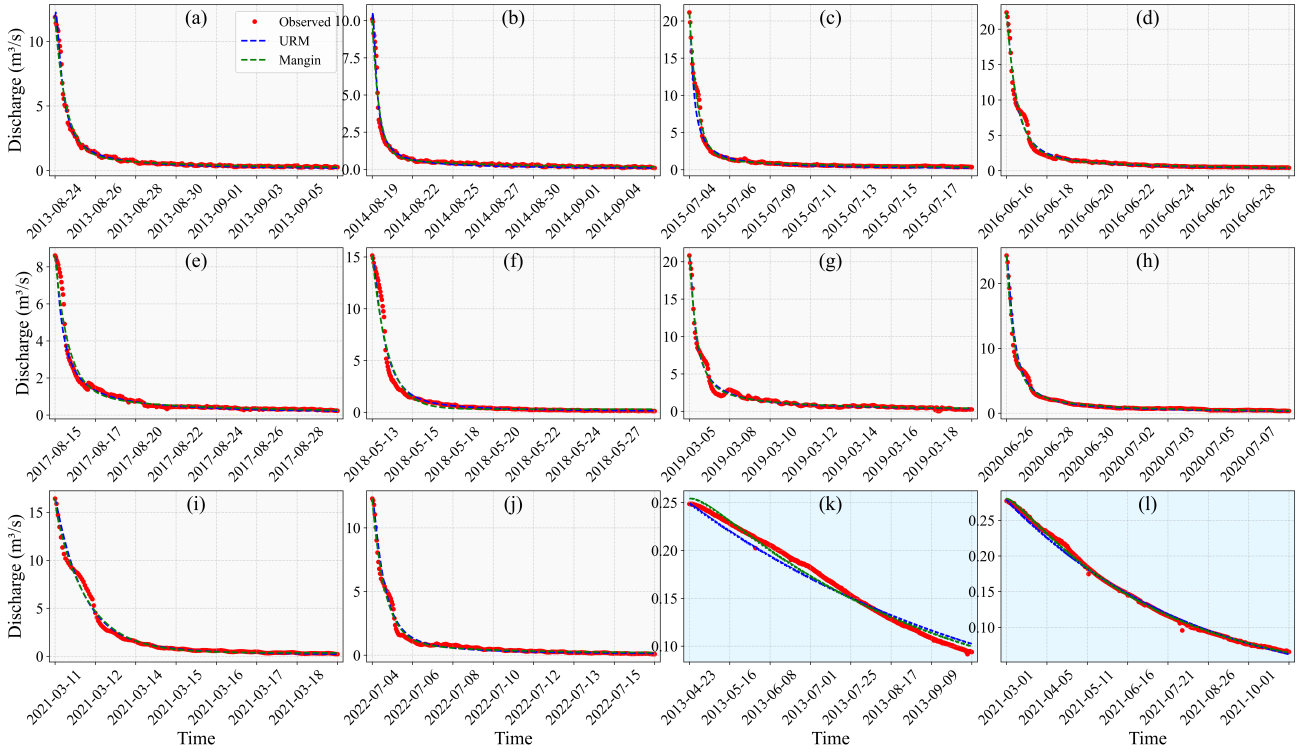

Figure 6. Observed and simulated recession curves for twelve recession events. Panels (a–j) show ten recession events from monsoon karst springs in southwest China; panels (k–l) show two recession events from Mediterranean karst springs in central Italy

https://doi.org/10.5194/egusphere-2025-6044
Preprint. Discussion started: 3 February 2026

For the two Italian events shown in Figure 6k–l (duration 3907–6003 h), both models perform excellently in simulating the prolonged, near-exponential recessions. The URM reaches a median KGE of 0.92 and RMSE of $0.006\ \mathrm{m^3 s^{-1}}$. Notably, the calibrated URM parameters converge to $n = 1$ and $\gamma \approx 0$, with α values on the order of $2.5\text{–}2.6 \times 10^{-4}$. This configuration corresponds to a linear reservoir behaviour, which emerges naturally from the unified model as a special case, demonstrating the model's adaptability to matrix-dominated flow regimes. This collapse toward $n \approx 1$ and $\gamma \approx 0$ indicates that these recessions are adequately described by a simpler limiting form of the URM (linear-reservoir behavior) rather than requiring all process terms to be active. Parameter identifiability and uncertainty supporting this interpretation are examined in Sect. 4.2.

The fitted URM parameters delineate the two regions clearly. For China, the nonlinearity exponent is tightly centred at $n \approx 2$, indicating pronounced early-time curvature consistent with efficient, turbulent conduit drainage; in Italy, both events yield $n = 1$, consistent with a linear storage–discharge relation. The drainage coefficient α also separates the regions: Chinese events span 0.01–0.03, whereas the Italian events are $2.5\text{–}2.6 \times 10^{-4}$, about two orders lower, implying much slower effective drainage. The exchange parameters γ and λ are required in China to sustain the recession tail, while the Italian fits converge to $\gamma/\lambda \approx 0$, rendering the tail indistinguishable from a single linear reservoir at the outlet(Table 2)

Table 2. Calibrated parameters and performance metrics for the URM and Mangin models ($\mathrm{m^3\ s^{-1}}$).

Spring	Index	Start time	Hours	URM						Mangin model						
				α	n	γ	λ	KGE	RMSE	q_{r0}	α	q_0	ε	η	KGE	RMSE
Zhaidi spring (China)	a	2013-08-24 08:00	353	0.02	2	3.02	0.32	0.97	0.14	10.15	0.07	1.73	0	0.02	0.94	0.22
	b	2014-08-19 22:00	427	0.03	2	3.99	0.44	0.91	0.16	9.10	0.10	0.99	0	0.01	0.93	0.20
	c	2015-07-04 15:00	374	0.01	2	4.55	0.65	0.85	0.52	19.28	0.09	1.87	0	0.01	0.99	0.27
	d	2016-06-16 09:00	339	0.01	2.1	4.34	0.20	0.98	0.38	17.92	0.08	4.46	0	0.03	0.98	0.38
	e	2017-08-15 21:00	353	0.01	2	0.96	0.56	0.85	0.29	6.88	0.06	1.73	0	0.02	0.92	0.25
	f	2018-05-13 14:00	382	0.02	1.98	4.03	0.12	0.93	0.45	15.03	0.05	0.10	1	0.35	0.91	0.51
	g	2019-03-05 23:00	350	0.01	2	3.31	0.59	0.99	0.34	12.81	0.11	8.02	0	0.05	0.97	0.36
	h	2020-06-26 19:00	298	0.01	2	5.76	0.32	0.94	0.40	12.83	0.13	11.48	0	0.10	0.97	0.34
	i	2021-03-11 19:00	189	0.03	2	7.39	0.11	0.97	0.40	14.78	0.05	1.65	0.21	1.00	0.99	0.35
	j	2022-07-04 11:00	319	0.02	2	3.55	0.16	0.95	0.25	10.44	0.07	1.86	0	0.03	0.97	0.21
Lupa spring (Italy)	k	2013-04-23 00:00	3907	0.00025	1	0	—	0.88	0.008	0.2542	0.0003	0	—	—	0.98	0.005
	l	2021-03-01 00:00	6003	0.00026	1	0	—	0.96	0.004	0.2805	0.0003	0	—	—	0.99	0.002

4.2 Regional patterns and transferability of URM parameters

Parameter identifiability and uncertainty were assessed using optimization-derived 95% confidence intervals for each recession event. This analysis evaluated the robustness of the calibrated parameters and their physical interpretability. The composite plots of α against n and γ against λ (Figure 7) reveal a well-defined regional separation, offering diagnostic insight into aquifer

https://doi.org/10.5194/egusphere-2025-6044
Preprint. Discussion started: 3 February 2026

behaviour. Confidence intervals for α and n are generally narrow across both regions, underscoring that the dominant drainage term is well constrained by the recession data. Even in the few Chinese events with comparatively wider intervals, the estimates remain consistent with $n \approx 2$, supporting a conduit-dominated early drainage regime. A similarly clear contrast is evident in the exchange parameters. For the Chinese springs, γ and λ are strictly positive and well-constrained in most events, corroborating the physically consistent interpretation of a persistent recession tail sustained by delayed exchange. In the Italian springs, the confidence intervals for both γ and λ straddle zero, indicating that these parameters are statistically indistinguishable from zero. This result is consistent with the observed near-exponential recessions, which do not require a separate exchange process to be represented at the spring outlet.

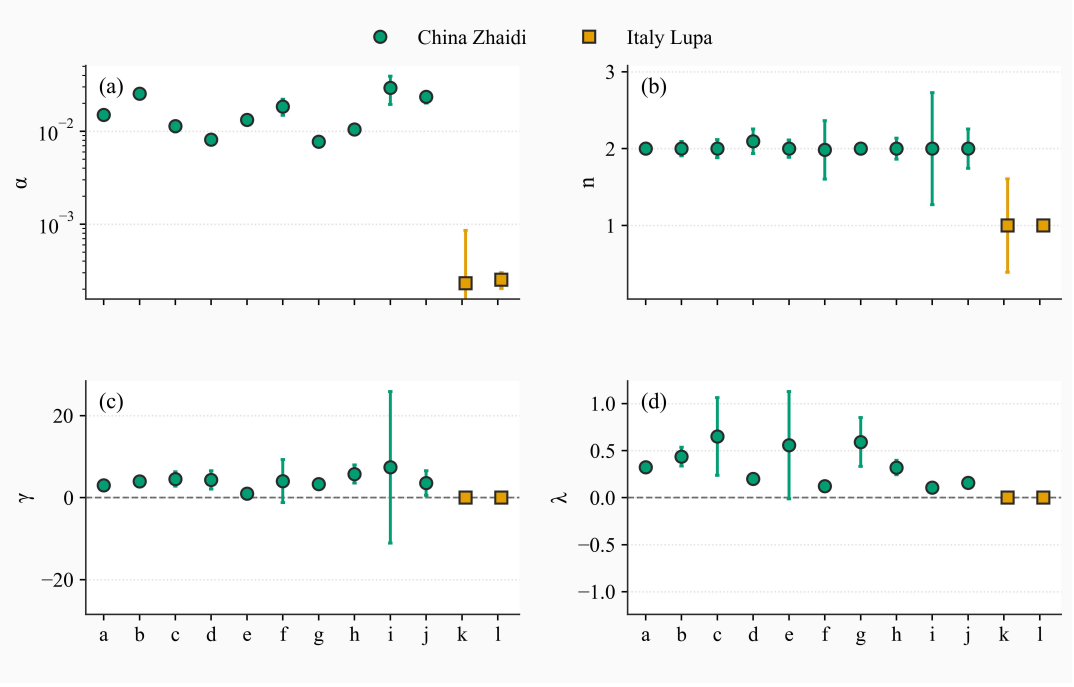

Figure 7. Event-wise uncertainty and regional contrasts in the drainage and exchange parameters for the unified recession model. Panels (a)–(d) show the fitted values and 95 % confidence intervals for α, n, γ, and λ, respectively

To assess whether the regional patterns of URM parameters also have predictive value, we constructed representative parameter sets for the two regions by averaging the well-constrained event-wise estimates (Sect. 4.1). For the Chinese Zhaidi spring this yields $\alpha = 0.015$, $n = 2$, $\gamma = 4.069$ and $\lambda = 0.239$, whereas the Italian Lupa spring is characterised by $\alpha = 2.5 \times 10^{-4}$, $n = 1$ and exchange parameters statistically indistinguishable from zero ($\gamma \approx 0$, $\lambda \approx 0$). These regional parameter sets were then used, without further calibration, to simulate two independent long drought recessions at the Zhaidi and Lupa springs. In each case the URM was initialised only with the observed discharge at the start of the event. Figure 8 illustrates the resulting simulations. For the Zhaidi spring the regional parameter set reproduces both the strong early-time curvature and the gradual transition to a near-linear tail, achieving a KGE of 0.80 and an RMSE of $0.38\ \mathrm{m^3\,s^{-1}}$. For the Lupa spring the regional configuration

https://doi.org/10.5194/egusphere-2025-6044
Preprint. Discussion started: 3 February 2026

effectively reduces to a linear reservoir and yields an almost perfect match to the observed near-exponential recession with a KGE of 0.97 and an RMSE of $0.004\ \mathrm{m^3\,s^{-1}}$. The good performance obtained without re-calibration confirms that the fitted URM parameters are not only diagnostic of conduit- and matrix-dominated regimes, but also transferable within each region for predicting independent drought recessions.

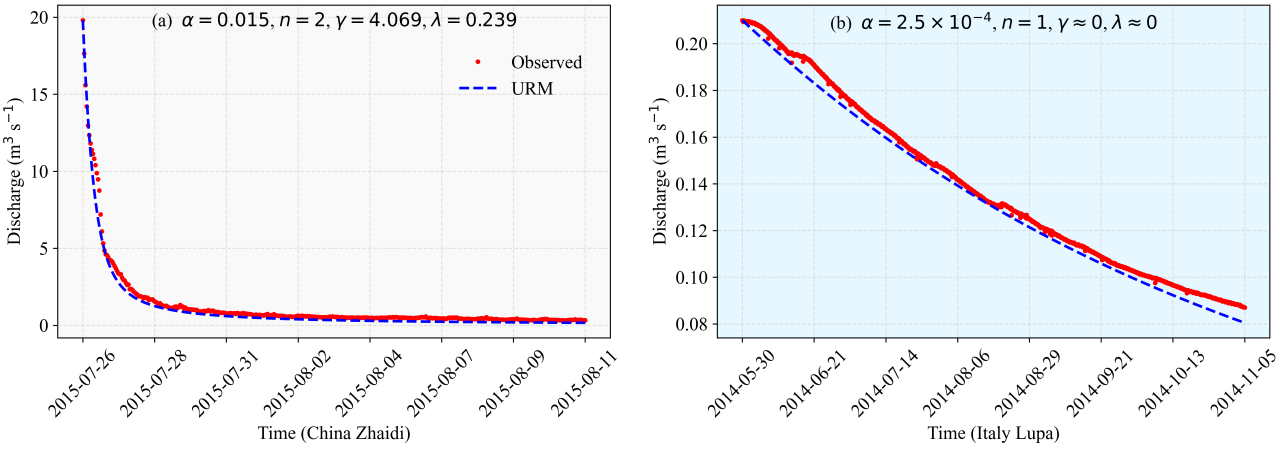

Figure 8. Regional parameter sets applied to two independent long drought recessions.

4.3 Regime classification and process interpretation in $(n, \tilde{S})$ space

In the URM, recession behavior can be summarized by the drainage nonlinearity exponent n and the dimensionless exchange ratio $\tilde{S} \equiv \gamma/(\lambda Q_0)$ (Sect. 2), which compares the cumulative exchange-input scale γ/λ to the event-specific discharge scale Q_0. Mapping events in the $(n, \tilde{S})$ space (Fig. 9) reveals distinct functional regimes of karst spring recession. We partition the diagram using the reference value $n = 1.5$, motivated by classical Boussinesq-type recession behavior, and the threshold $\tilde{S} = 1$, which marks the transition where the integrated exchange contribution becomes comparable to Q_0. The lower-left quadrant ($\tilde{S} < 1$, $n \approx 1$) corresponds to near-linear, matrix-dominated drainage; the upper-left ($\tilde{S} > 1$, $n \approx 1$) indicates linear drainage with a pronounced exchange-sustained tail; the lower-right ($\tilde{S} < 1$, $n > 1.5$) represents nonlinear conduit-dominated drainage with strong early-time curvature and negligible tailing; and the upper-right ($\tilde{S} > 1$, $n > 1.5$) reflects mixed control, where nonlinear conduit drainage coexists with substantial delayed exchange. Classical recession models occupy specific regions within this phase space. The Maillet (1905) model corresponds to the linear limit at $n = 1$, $\tilde{S} = 0$, positioned near the lower-left edge. Models such as Wittenberg (1999), Coutagne (1948), and Drogue (1972) fall within the lower-right domain ($\tilde{S} = 0, n > 1.5$), expressing enhanced early-time curvature due to conduit effects. The Boussinesq (1903) solution lies along the boundary at $n = 1.5$, $\tilde{S} = 0$. Multi-reservoir and multi-exponential formulations—including early developments by Barnes (1939) and Schoeller (1948), along with widely used variants by Mangin (1975), Kullman (2000), and Basha (2020)—plot in the upper-left quadrant ($\tilde{S} > 1$), reflecting linear behaviour with notable delayed exchange that sustains the recession tail. In the URM, the delayed matrix-to-conduit contribution is represented by a single exponential exchange kernel, $\gamma e^{-\lambda t}$. If needed, this term can

https://doi.org/10.5194/egusphere-2025-6044
Preprint. Discussion started: 3 February 2026

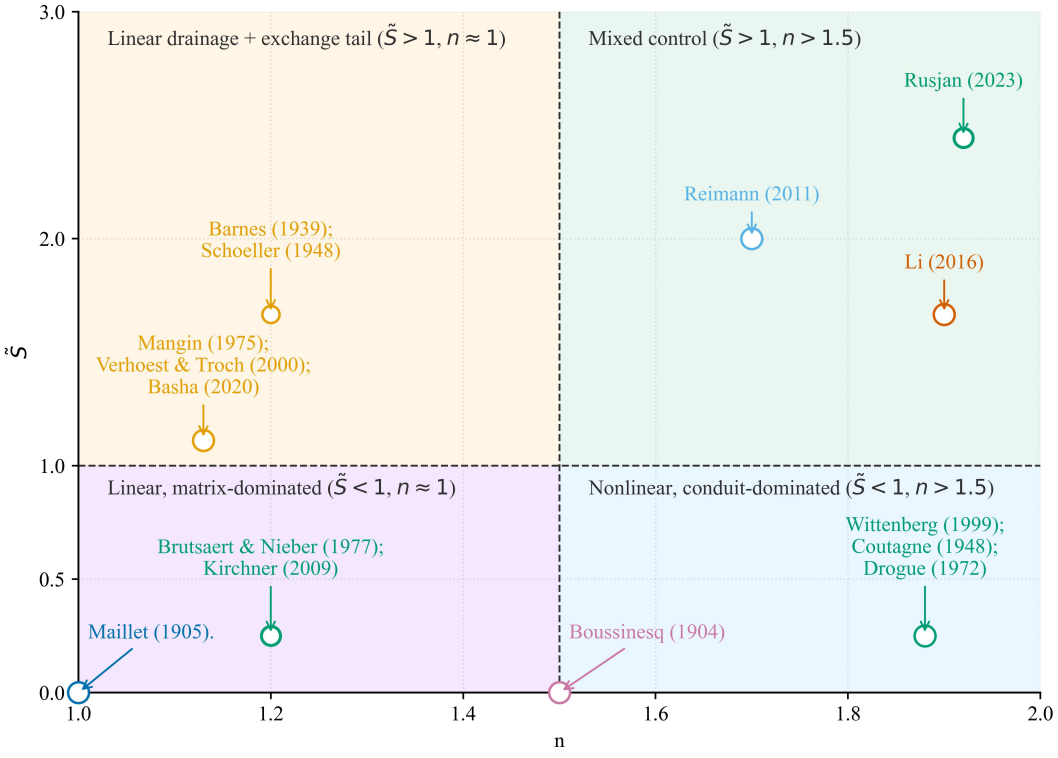

Figure 9. Classification of karst spring recession behaviour in the unified parameter space $(n, \tilde{S})$.

be extended phenomenologically to a finite superposition of exponentials, $\sum_{i=1}^{k} \gamma_i e^{-\lambda_i t}$, to emulate multi-timescale delayed release and to connect with classical multi-exponential recession representations (Barnes, 1939; Schoeller, 1948). Process-based models that explicitly represent nonlinear conduit resistance and conduit–matrix exchange (Reimann et al., 2011) motivate the mixed-control interpretation of the upper-right region ($n > 1.5$ and $\tilde{S} > 1$), where nonlinear conduit drainage coexists with substantial delayed exchange/storage effects. Complementary data-driven diagnostics of karst recession dynamics are provided by dynamical-systems approaches (Rusjan et al., 2023). Brutsaert and Nieber (1977) and Kirchner (2009) provide diagnostic recession frameworks that focus on a single-valued relation between $\mathrm{d}Q/\mathrm{d}t$ and Q, which is captured in the URM when the exchange-input term is negligible ($\tilde{S} \ll 1$). Recession behaviour is analysed in the URM-based $(n, \tilde{S})$ diagnostic parameter space. In this space, many classical recession formulations appear as limiting cases or approximations under specific parameter constraints (Table 1), forming a continuous range of nonlinearity (the horizontal axis) and delayed exchange/storage influence (the vertical axis). The four URM parameters in Eq. (1) retain clear physical interpretations, thereby providing a single mechanistic framework that explains the emergence of different recession laws within this space.

To summarize the regime interpretation implied by the $(n, \tilde{S})$ mapping, Fig. 10 provides a schematic synthesis linking parameter space to qualitative process behaviour. The horizontal axis summarizes the structural continuum from matrix-dominated (poorly developed conduits) to conduit-dominated drainage, while the vertical axis indicates increasing recession steepness (shorter hydrological memory). The three shaded regions correspond to matrix-influenced, mixed conduit–matrix,

https://doi.org/10.5194/egusphere-2025-6044
Preprint. Discussion started: 3 February 2026

and conduit-dominated regimes identified in the $(n, \tilde{S})$ diagnostic space. The schematic highlights how regional contrasts (Mediterranean vs. monsoon settings) can be interpreted as shifts between these regimes, providing an intuitive bridge from calibrated URM parameters to process-based discussion.

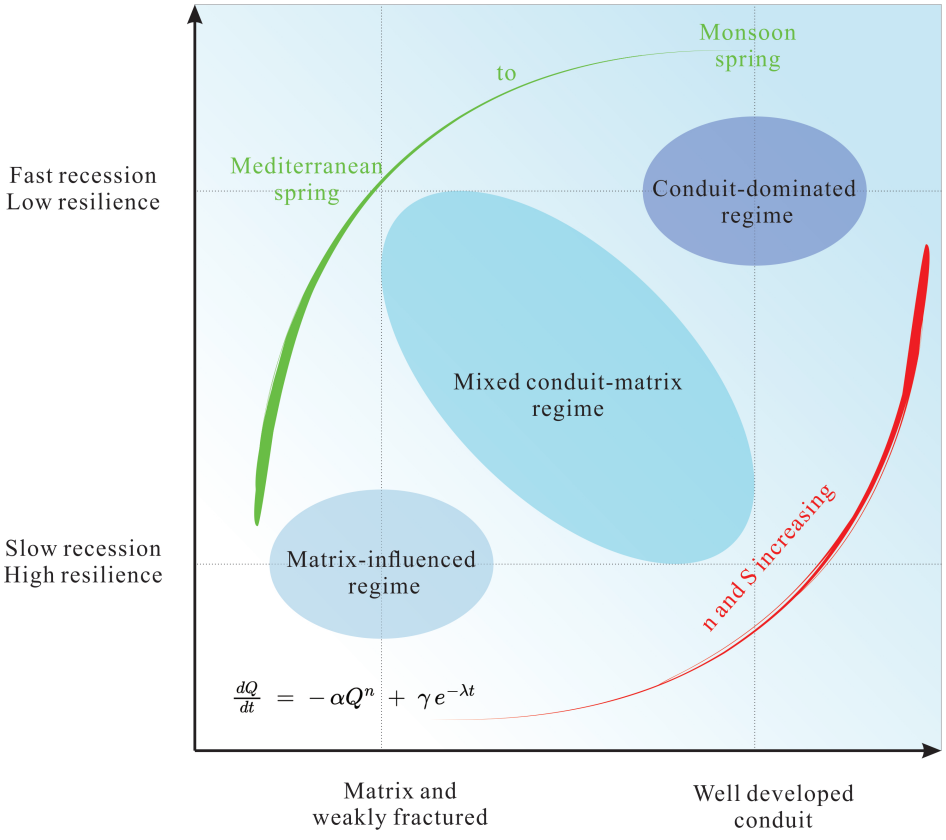

Figure 10. Schematic synthesis of recession regimes implied by the URM parameters, linking the $(n, \tilde{S})$ diagnostic space to qualitative drainage regimes (matrix-influenced, mixed, and conduit-dominated).

4.4 Implications for drought resilience and water resources

Figure 11 illustrates how contrasting parameter regimes translate into different depletion trajectories and, consequently, different levels of drought resilience. The curves show normalised discharge Q/Q_0 for two representative parameter sets of the unified recession model: a conduit-dominated case ($n = 2$ and relatively large α; red) and a matrix-influenced case ($n = 1$ and much smaller α; green). The shaded region between the curves denotes a transition regime with intermediate depletion times. To make these regime implications more quantitative, we define an operational depletion time t_θ as the time required for the normalised discharge to drop to a management-relevant threshold, $Q(t_\theta) = \theta Q_0$. When present, the exponentially decaying exchange input is characterised by the relaxation time $\tau_{ex} = 1/\lambda$.

https://doi.org/10.5194/egusphere-2025-6044
Preprint. Discussion started: 3 February 2026

Neglecting exchange in the early drainage phase yields the analytical approximation

$$t_\theta^{(d)} \approx \begin{cases} \dfrac{\theta^{1-n}-1}{(n-1)\alpha Q_0^{n-1}}, & n \neq 1, \\ \dfrac{\ln(1/\theta)}{\alpha}, & n = 1, \end{cases}$$

which provides a reference depletion time scale for the drainage term. In the full URM, the numerically evaluated t_θ (shown as $t_{0.2}$ in Fig. 11) is expected to increase with the dimensionless exchange ratio $\tilde{S} = \gamma/(\lambda Q_0)$, reflecting the growing importance of delayed exchange in sustaining the recession tail.

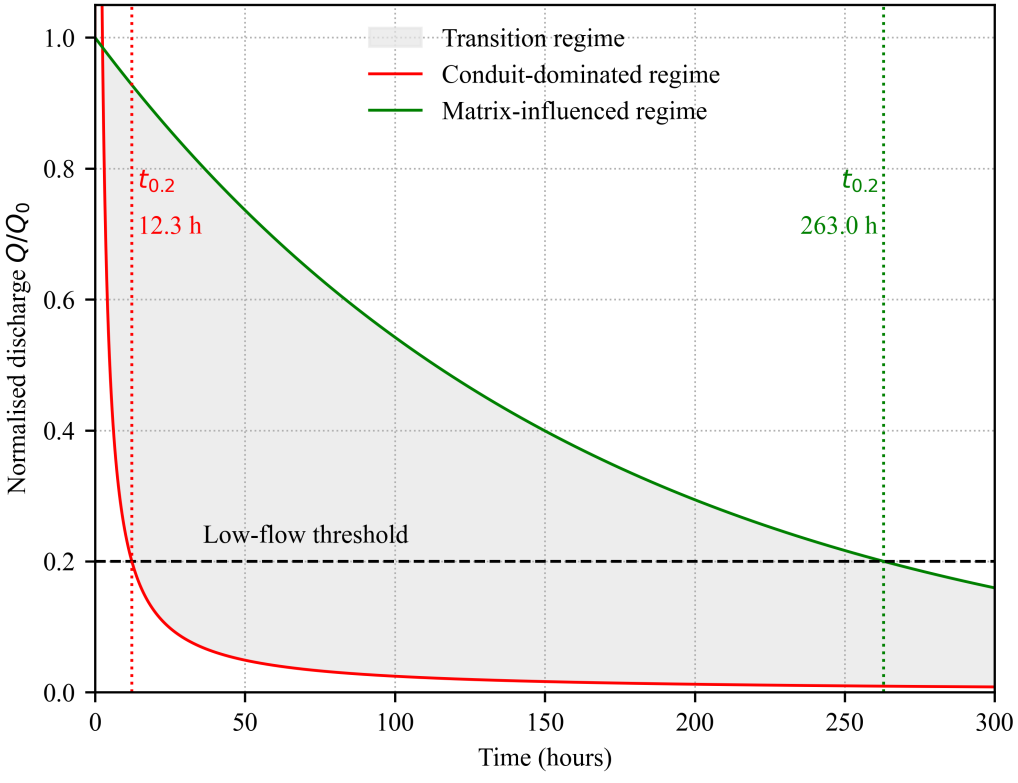

Figure 11. Typical normalised recession curves Q/Q_0 derived from the URM. The dashed line indicates the low-flow threshold $\theta = 0.2$ used to define the depletion time $t_{0.2}$.

Together with the functional regimes defined in the $(n, \tilde{S})$ space, the depletion time $t_{0.2}$ provides a practical, comparable metric of drought-relevant spring behaviour. In Fig. 11, the conduit-dominated parameter set reaches the low-flow threshold rapidly ($t_{0.2} \approx 12\,\mathrm{h}$), whereas the matrix-influenced set sustains discharge for much longer ($t_{0.2} \approx 263\,\mathrm{h}$), consistent with higher hydrological memory. Because URM parameters can be estimated from discharge records alone, this framework offers a first-order screening tool where subsurface information is scarce. Repeated calibration over time could track shifts in n, α and $\tilde{S}$

https://doi.org/10.5194/egusphere-2025-6044
Preprint. Discussion started: 3 February 2026

as indicators of changing recharge conditions, abstraction pressure or land-use change, linking observed recession dynamics to drought management from catchment to regional scales.

4.5 Methodological implications, limitations and outlook

The unified recession model provides a compact way of linking karst spring hydrographs to subsurface processes, while raising several methodological considerations. By embedding nonlinear conduit drainage and matrix contribution within a single analytical expression, the model avoids fitting separate equations to different portions of the recession limb and enables direct comparison across events and sites within a consistent parameter space. This compact parameterisation is particularly useful for cross-regional analyses and for settings where discharge data are available but additional subsurface information is limited.

At the same time, the present analysis is confined to relatively short, event-scale recessions and does not explicitly account for interactions with seasonal groundwater-level variations, pumping, or surface–groundwater exchange. These limitations motivate future work coupling the recession framework with simple recharge representations or long-term groundwater-level observations to bridge event-scale dynamics and multi-year variability. More generally, the URM is not intended to replace distributed models, but to complement them—for example as a benchmark for emergent recession behaviour, a guide for targeted field campaigns, or a first-order diagnostic of aquifer functioning. Extending the framework to include solute, temperature, or tracer information may provide additional constraints on conduit–matrix interactions and refine process interpretation.

5 Conclusions

A unified recession model (URM) provides a continuous description of karst spring recessions without subjective segmentation of the early-time decline and late-time tail. The model links recession shape to four interpretable parameters that represent nonlinear conduit drainage and delayed matrix contribution, thereby placing several classical recession formulations within a common limiting-case framework.

Across contrasting karst settings in southwest China and central Italy, URM reproduces event-scale recessions and improves upon the two-component benchmark. Calibrated parameters reveal systematic regional contrasts: the Chinese spring is characterised by strongly nonlinear, conduit-dominated drainage ($n \approx 2$ and relatively large α) with a measurable delayed contribution, whereas the Italian spring exhibits quasi-linear depletion consistent with matrix-influenced behaviour ($n \approx 1$ and negligible exchange contribution). Event-to-event uncertainty analysis indicates that these contrasts are robust rather than driven by individual recessions.

Mapping recessions in the URM diagnostic space $(n, \tilde{S})$ delineates functional regimes ranging from matrix-influenced to mixed and conduit-dominated behaviour. This regime view links observable hydrograph shape to subsurface functioning and yields drought-relevant metrics such as operational depletion time. Because the URM can be estimated from discharge records alone, it offers a practical screening tool in data-scarce regions and a parsimonious component for larger-scale hydrological and Earth system applications. Future work should extend the framework beyond event-scale recessions by accounting for seasonal

https://doi.org/10.5194/egusphere-2025-6044
Preprint. Discussion started: 3 February 2026

groundwater fluctuations, pumping and recharge dynamics, and by integrating complementary constraints from groundwater levels, tracers or temperature.

Appendix A: Derivation to a single ODE and parameter meanings

The spring discharge $Q(t)\,[L^3/T]$ reflects both rapid drainage from the conduit and delayed contributions from the matrix. Conduit flow is governed by a Forchheimer-type relationship that captures both laminar and turbulent regimes (e.g. Mayaud et al., 2015). The hydraulic head in the conduit, $h_c\,[L]$, is expressed as a function of discharge:

$$h_c = L\big(aQ + bQ^2\big) \;\Rightarrow\; \frac{\mathrm{d}h_c}{\mathrm{d}t} = L\big(a + 2bQ\big)\,\frac{\mathrm{d}Q}{\mathrm{d}t}, \tag{A1}$$

where $L\,[L]$ is the conduit length, and a, b are coefficients representing linear and nonlinear resistance terms, respectively.

Matrix drainage and storage are jointly described by a lumped conduit–matrix exchange term. We define the exchange flux Q_{ex} as positive for flow from the matrix to the conduit and write

$$S_m\,\frac{\mathrm{d}h_m}{\mathrm{d}t} = -\,Q_{\mathrm{ex}}, \qquad Q_{\mathrm{ex}} = \sigma K_m\,(h_m - h_c) \tag{A2}$$

where $h_m\,[L]$ is the matrix hydraulic head, S_m is an effective matrix storage coefficient (matrix volume per unit head change), $K_m\,[L/T]$ is the matrix hydraulic conductivity, and σ is a lumped conductance parameter controlling the intensity of conduit–matrix exchange (e.g. Kovács and Sauter, 2007; Bailly-Comte et al., 2010). In this lumped formulation, Q_{ex} is a volumetric exchange discharge at the conduit scale.

The conduit storage follows a nonlinear power-law relation:

$$V = \kappa\,h_c^{\phi} \;\Rightarrow\; \frac{\mathrm{d}V}{\mathrm{d}t} = \kappa\,\phi\,h_c^{\phi-1}\,\frac{\mathrm{d}h_c}{\mathrm{d}t}, \tag{A3}$$

where $V\,[L^3]$ is the stored water volume in the conduit, κ is a geometry-dependent parameter, and ϕ characterizes the nonlinearity of the storage.

Applying the water balance in the conduit, the rate of change in conduit storage equals the net inflow:

$$\frac{\mathrm{d}V}{\mathrm{d}t} \;=\; -\,Q(t) + Q_{\mathrm{ex}}. \tag{A4}$$

Substituting Eqs. (A1)–(A3) into Eq. (A4) and transforming all variables to a discharge-based form, we introduce the head difference $\delta(t) = h_m - h_c$. From Eq. (A2) we obtain

$$\frac{\mathrm{d}\delta}{\mathrm{d}t} \;=\; \frac{\mathrm{d}h_m}{\mathrm{d}t} - \frac{\mathrm{d}h_c}{\mathrm{d}t} \;=\; -\,\frac{\sigma K_m}{S_m}\,(h_m - h_c) - \frac{\mathrm{d}h_c}{\mathrm{d}t} \;=\; -\,\lambda\,\delta - \frac{\mathrm{d}h_c}{\mathrm{d}t},$$

with $\lambda = \sigma K_m / S_m$. During late-time recession we assume that the temporal variation of the conduit head $h_c(t)$ is slow compared to the relaxation of the head difference, so that the term $-\mathrm{d}h_c/\mathrm{d}t$ can be neglected to leading order. Under this assumption, the head difference is taken to decay as

$$\frac{\mathrm{d}\delta}{\mathrm{d}t} = -\,\lambda\,\delta, \qquad \lambda = \frac{\sigma K_m}{S_m}, \tag{A5}$$

https://doi.org/10.5194/egusphere-2025-6044
Preprint. Discussion started: 3 February 2026

with solution $\delta(t) = \delta_0 \, \mathrm{e}^{-\lambda t}$, where δ_0 is the initial head difference. The parameter $\lambda\,[1/T]$ thus represents the characteristic decay rate of matrix–conduit head disequilibrium (e.g. Bailly-Comte et al., 2010)

Substituting the time-varying exchange term $Q_{\mathrm{ex}}(t) = \sigma K_m \delta_0 \, \mathrm{e}^{-\lambda t}$ into Eq. (A4) yields the discharge evolution equation

$$\frac{\mathrm{d}Q}{\mathrm{d}t} \;=\; -\,\frac{Q - \sigma K_m \delta_0 \, \mathrm{e}^{-\lambda t}}{D(Q)}, \tag{A6}$$

where the damping function

$$D(Q) \;=\; \kappa\,\phi\,L^{\phi}\big(aQ + bQ^2\big)^{\phi-1}\big(a + 2bQ\big) + \frac{S_m}{L\big(a + 2bQ\big)} \tag{A7}$$

collects the contributions of conduit storage, inertial flow resistance and matrix storage.

Here, $D(Q)$ represents an effective hydraulic resistance, parameterized by conduit geometry L, inertial flow properties a, b, matrix storage S_m, and the nonlinear exponent ϕ. To derive a tractable lumped model, we conduct an asymptotic analysis of $D(Q)$ across characteristic flow regimes (high- and low-flow limits). In high-flow conditions $\big(Q \gg \sqrt{a/b}\big)$, the nonlinear Forchheimer term dominates and the damping function simplifies to

$$D(Q) \approx 2\,\kappa\,\phi\,L^{\phi}\,b^{\phi}\,Q^{2\phi-1},$$

while the matrix contribution becomes negligible. In contrast, under low-flow conditions $\big(Q \ll \sqrt{a/b}\big)$, the system behaves linearly and matrix storage dominates, yielding

$$D(Q) \approx \frac{S_m}{La}.$$

By asymptotically matching these limits, the leading-order term $Q/D(Q)$ can be approximated by a power-law expression αQ^n, in the spirit of classical nonlinear recession analysis (e.g. Brutsaert and Nieber, 1977; Rupp and Selker, 2006). Likewise, over the characteristic time scale $1/\lambda$ we assume that the variation of $D(Q)$ is moderate compared to the exponential decay of $\delta(t)$, so that the delayed matrix–conduit exchange term

$$\frac{\sigma K_m \delta_0 \, \mathrm{e}^{-\lambda t}}{D(Q)}$$

can be approximated as $\gamma\,\mathrm{e}^{-\lambda t}$. We thus obtain the final recession equation:

$$\frac{\mathrm{d}Q}{\mathrm{d}t} \;=\; -\alpha Q^n \;+\; \gamma\,\mathrm{e}^{-\lambda t}. \tag{A8}$$

This unified model, integrating a nonlinear term $\big(-\alpha Q^n\big)$ and an exponential tailing input $\big(\gamma\,\mathrm{e}^{-\lambda t}\big)$ to describe complex recession dynamics, is henceforth referred to as the unified recession model (URM), extending the classical nonlinear recession framework of Brutsaert and Nieber (1977) with an explicit matrix–conduit exchange term.

Author contributions. Liangjie Zhao: Conceptualization & original draft; Yang Yang: Writing & software; Stefano Fazi: Review; Song Luan: Investigation & methodology; Cheng Li: Validation; Ning Zhang: Review; Elisabetta Preziosi: Conceptualization & data

https://doi.org/10.5194/egusphere-2025-6044
Preprint. Discussion started: 3 February 2026

Table A1. List of symbols used in the unified recession model (URM).

Symbol	Description	Units / notes
t	Time	T
$Q(t)$	Spring discharge (outlet)	L^3T^{-1}
Q_0	Initial discharge scale for normalisation	L^3T^{-1}
h_c	Conduit hydraulic head	L
h_m	Matrix hydraulic head	L
δ	Matrix–conduit head difference ($h_m - h_c$)	L
Δh	Along-conduit head drop (upstream–downstream)	L
J	Hydraulic gradient (1-D mean: $J \approx \Delta h/L$)	dimensionless
V	Stored water volume in the conduit	L^3
L	Conduit length	L
K_m	Matrix hydraulic conductivity	LT^{-1}
S_m	Effective matrix storage coefficient	lumped (volume per unit head)
σ	Matrix–conduit exchange conductance	lumped parameter
Q_{ex}	Matrix–conduit exchange discharge	L^3T^{-1} (lumped)
a, b	Linear / quadratic head-loss coefficients	
κ	Conduit storage geometry factor	lumped storage parameter
ϕ	Storage nonlinearity exponent	dimensionless
λ	Exchange relaxation rate	T^{-1}
α	Nonlinear drainage coefficient	$L^{3(1-n)}T^{n-2}$
n	Recession exponent	dimensionless
γ	Amplitude of exponential exchange input	L^3T^{-2}
$\tilde{S}$	Dimensionless exchange ratio, $\tilde{S} \equiv \gamma/(\lambda Q_0)$	dimensionless

Competing interests. The authors declare that they have no known competing financial interests or personal relationships that could have appeared to influence the work reported in this paper.

Acknowledgements. This research was supported by the National Key Research and Development Program of China (Grant Nos. 2024YFC3713001 and 2023YFB3907703_05), the Karst Water Resources and Environment Academician Workstation of Guizhou Province (Qiankehepingtai-KXJZ[2024]005), and the Guizhou Province Leading Research Team on Geothermal Water and Mineral Resources (Qiankeherencai-CXTD[2025]003)

https://doi.org/10.5194/egusphere-2025-6044
Preprint. Discussion started: 3 February 2026

References

Abirifard, M., Birk, S., Raeisi, E., et al.: Dynamic volume in karst aquifers: Parameters affecting the accuracy of estimates from recession analysis, Journal of Hydrology, 612, 128 286, 2022.

Bailly-Comte, V., Martin, J. B., Jourde, H., and Screaton, E. J.: Water exchange and pressure transfer between conduits and matrix and their influence on hydrodynamics of two karst aquifers with sinking streams, Journal of Hydrology, 386, 55–66, https://doi.org/10.1016/j.jhydrol.2010.03.005, 2010.

Barnes, B. S.: The structure of discharge–recession curves, Transactions, American Geophysical Union, 20, 721–725, 1939.

Basha, H. A.: Flow recession equations for karst systems, Water Resources Research, 56, e2020WR027 384, 2020.

Bauer, S., Liedl, R., and Sauter, M.: Modeling of karst aquifer genesis: Influence of exchange flow, Water Resources Research, 39, 1285, 2003.

Bear, J.: Dynamics of Fluids in Porous Media, American Elsevier, New York, 1972.

Boussinesq, V. J.: Recherches théoriques sur l'écoulement des nappes d'eau infiltrées dans le sol et sur le débit des sources, Journal de Mathématiques Pures et Appliquées, 10, 5–78, https://eudml.org/doc/235283, 1904.

Brutsaert, W. and Nieber, J. L.: Regionalized drought flow hydrographs from a mature glaciated plateau, Water Resources Research, 13, 637–643, https://doi.org/10.1029/WR013i003p00637, 1977.

Çallı, K. Ö. and Hartmann, A.: A comparative evaluation of automated recession extraction procedures for karst spring hydrographs, Turkish Journal of Water Science and Management, 6, 2–30, 2022.

Çelik, M., Çallı, S. S., Altın, S., et al.: Reducing climate impacts on karst groundwater resources by constructing a cave dam: A case study from Central Taurus Karst, Türkiye, Journal of Hydrology, 636, 131 245, 2024.

Cerino Abdin, E., Taddia, G., Gizzi, M., and Lo Russo, S.: Reliability of spring recession curve analysis as a function of the temporal resolution of the monitoring dataset, Environmental Earth Sciences, 80, 249, 2021.

Chang, W., Wan, J., Tan, J., et al.: Responses of spring discharge to different rainfall events for single-conduit karst aquifers in Western Hunan Province, China, International Journal of Environmental Research and Public Health, 18, 5775, 2021.

Chen, Y. F., Zhou, J. Q., Hu, S. H., et al.: Evaluation of Forchheimer equation coefficients for non-Darcy flow in deformable rough-walled fractures, Journal of Hydrology, 529, 993–1006, 2015.

Chin, D. A., Price, R. M., and DiFrenna, V. J.: Nonlinear flow in karst formations, Groundwater, 47, 669–674, 2009.

Cinkus, G., Mazzilli, N., and Jourde, H.: KarstID: an R Shiny application for the analysis of karst spring discharge time series and the classification of karst system hydrological functioning, Environmental Earth Sciences, 82, 136, 2023.

Coutagne, A.: Météorologie et hydrologie. Étude générale des débits et des facteurs qui les conditionnent. 2ème partie: Les variations de débit en période non influencée par les précipitations. Le débit d'infiltration (corrélations fluviales internes), La Houille Blanche, pp. 416–436, https://doi.org/10.1051/lhb/1948053, 1948.

Dong, Y., Li, Y., Fu, Y., et al.: Influence of precipitation on the estimation of karstic water storage variation, Water, 17, 986, 2025.

Drogue, C.: Analyse statistique des hydrogrammes de décrues des sources karstiques, Journal of Hydrology, 15, 49–68, 1972.

Elhanati, D., Goeppert, N., and Berkowitz, B.: Karst aquifer discharge response to rainfall interpreted as anomalous transport, Hydrology and Earth System Sciences, 28, 4239–4249, https://doi.org/10.5194/hess-28-4239-2024, 2024.

Fatoni, H., Kholis, A. N., Kurniawan, I. A., et al.: Use of discharge variability, aquifer memory effect, and recession curve analysis in several springs to characterize karst aquifers in the tropical area, Geosciences Journal, 28, 925–939, 2024.

https://doi.org/10.5194/egusphere-2025-6044
Preprint. Discussion started: 3 February 2026

Fauzi, D. R., Adji, T. N., Setyawan, A., et al.: Analysis of floods recession constant of several karst springs in the north side of Karangbolong (Gombong) karst area, Central Java, in: AIP Conference Proceedings, vol. 2363, 2021.

Fiorillo, F.: The recession of spring hydrographs, focused on karst aquifers, Water Resources Management, 28, 1781–1805, 2014.

Ford, D. C. and Williams, P. W.: Karst Hydrogeology and Geomorphology, John Wiley & Sons, Chichester, 2007.

Gan, R. and Luo, Y.: Using the nonlinear aquifer storage–discharge relationship to simulate the base flow of glacier- and snowmelt-dominated basins in northwest China, Hydrology and Earth System Sciences, 17, 3577–3586, 2013.

Geravand, F., Hosseini, S. M., Maghsoudi, M., et al.: Characterization of karst springs from Zagros Mountain in southwestern Iran, Environmental Earth Sciences, 81, 529, 2022.

Ghotbi, S., Wang, D., Singh, A., et al.: Climate and landscape controls of regional patterns of flow duration curves across the continental United States: Statistical approach, Water Resources Research, 56, e2020WR028 041, 2020.

Giese, M., Caballero, Y., Hartmann, A., and Charlier, J.-B.: Trends in long-term hydrological data from European karst areas: insights for groundwater recharge evaluation, Hydrology and Earth System Sciences, 29, 3037–3054, https://doi.org/10.5194/hess-29-3037-2025, 2025.

Guo, X., Li, J., Zeng, Y., et al.: A theoretical model for simulating periodic processes of intermittent karst springs considering changed recharge rates into siphon cavity, Journal of Hydrology, 617, 129 017, 2023.

Hartmann, A., Goldscheider, N., Wagener, T., Lange, J., and Weiler, M.: Karst water resources in a changing world: Review of hydrological modeling approaches, Reviews of Geophysics, 52, 218–242, https://doi.org/10.1002/2013RG000443, 2014.

Jachens, E. R., Rupp, D. E., Roques, C., et al.: Recession analysis revisited: Impacts of climate on parameter estimation, Hydrology and Earth System Sciences, 24, 1159–1170, 2020.

Kale, R. V., Dwivedi, A. K., Ojha, C. S. P., et al.: Evaluation of spring flows using recession flow analysis techniques, Water Supply, 24, 2232–2246, 2024.

Kirchner, J. W.: Catchments as simple dynamical systems: Catchment characterization, rainfall–runoff modeling, and doing hydrology backward, Water Resources Research, 45, W02 429, 2009.

Klammler, H., Jawitz, J. W., and Cohen, M. J.: A simple model of flow reversals in Florida's karst springs, Water Resources Research, 60, e2023WR035 987, 2024.

Kovács, A. and Sauter, M.: Modelling karst hydrodynamics, in: Methods in Karst Hydrogeology, edited by Goldscheider, N. and Drew, D., vol. 26 of *IAH International Contributions to Hydrogeology*, pp. 201–222, Taylor & Francis/Balkema, London, ISBN 978-0-415-42873-6, 2007.

Li, G., Goldscheider, N., and Field, M. S.: Modeling karst spring hydrograph recession based on head drop at sinkholes, Journal of Hydrology, 542, 820–827, 2016.

Maillet, E.: Essais d'hydraulique souterraine et fluviale, A. Hermann, Paris, https://archive.org/details/essaisdhydrauli00mailgoog, 218 pp., 1905.

Mangin, A.: Contribution à l'étude hydrodynamique des aquifères karstiques. 3ème partie: Constitution et fonctionnement des aquifères karstiques, Annales de Spéléologie, 30, 21–124, 1975.

Mayaud, C., Walker, P., Hergarten, S., and Birk, S.: Nonlinear Flow Process: A New Package to Compute Nonlinear Flow in MODFLOW, Groundwater, 53, 645–650, https://doi.org/10.1111/gwat.12243, 2015.

Michel, C., Perrin, C., and Andréassian, V.: The exponential store: a correct formulation for rainfall–runoff modelling, Hydrological Sciences Journal, 48, 109–124, 2003.

https://doi.org/10.5194/egusphere-2025-6044
Preprint. Discussion started: 3 February 2026

Mujib, M. A., Adji, T. N., Haryono, E., et al.: Karst aquifer characterization by means of its karstification degree and time series analysis (Case: Ngerong Spring in Rengel Karst, East Java, Indonesia), Indonesian Journal on Geoscience, 11, 45–60, 2024.

Olarinoye, T., Gleeson, T., Marx, V., et al.: Global karst springs hydrograph dataset for research and management of the world's fastest-flowing groundwater, Scientific Data, 7, 59, 2020.

Pansa, A., Butera, I., Gómez-Hernández, J. J., et al.: Predicting discharge from a complex karst system using the ensemble smoother with multiple data assimilation, Stochastic Environmental Research and Risk Assessment, 37, 185–201, 2023.

Preziosi, E., Guyennon, N., Petrangeli, A. B., Romano, E., and Di Salvo, C.: A stepwise modelling approach to identifying structural features that control groundwater flow in a folded carbonate aquifer system, Water, 14, 2475, 2022.

Regione Umbria: Servizio idrografico regionale, https://www.regione.umbria.it/ambiente/servizio-idrografico, last access: 10 November 2025.

Reimann, T. and Hill, M. E.: MODFLOW–CFP: A new conduit flow process for MODFLOW–2005, Ground Water, 47, 321–325, 2009.

Reimann, T., Rehrl, C., Shoemaker, W. B., Geyer, T., and Birk, S.: The significance of turbulent flow representation in single–continuum models, Water Resources Research, 47, W09 503, 2011.

Rupp, D. E. and Selker, J. S.: On the use of the Boussinesq equation for interpreting recession hydrographs from sloping aquifers, Water Resources Research, 42, W12 421, https://doi.org/10.1029/2006WR005080, 2006.

Rusjan, S., Lebar, K., and Bezak, N.: Insight into heterogeneous karst catchment by the dynamical system approach, Advances in Water Resources, 180, 104 524, 2023.

Schoeller, H.: Le régime hydrogéologique des calcaires éocènes du synclinal du Dyr el Kef (Tunisie), Bulletin de la Société Géologique de France, 18, 167–180, sér. 5, 1948.

Schuler, P., Duran, L., Johnston, P., et al.: Quantifying and numerically representing recharge and flow components in a karstified carbonate aquifer, Water Resources Research, 56, e2020WR027 717, 2020.

Şen, Z.: General modeling of karst spring hydrographs and development of a dimensionless karstic hydrograph concept, Hydrogeology Journal, 28, 549–559, 2020.

Shirafkan, M., Mohammadi, Z., Sivelle, V., et al.: The effects of exchange flow on the karst spring hydrograph under the different flow regimes: A synthetic modeling approach, Water, 13, 1189, 2021.

Shirafkan, M., Mohammadi, Z., Kavousi, A., et al.: Toward the estimation of the transfer coefficient in karst systems: Using baseflow recession coefficient under matrix-restrained flow regime, Journal of Hydrology, 620, 129 441, 2023.

Sivelle, V. and Jourde, H.: A methodology for the assessment of groundwater resource variability in karst catchments with sparse temporal measurements, Hydrogeology Journal, 29, 137–157, 2021.

Sivelle, V., Cinkus, G., Mazzilli, N., Labat, D., Arfib, B., Massei, N., Cousquer, Y., Bertin, D., and Jourde, H.: Improvement of the KarstMod modelling platform for a better assessment of karst groundwater resources, Hydrology and Earth System Sciences, 29, 1259–1276, https://doi.org/10.5194/hess-29-1259-2025, 2025.

Teixeira, G. M., de Paula, R. S., Velasquez, L. N. M., et al.: Evaluation of recharge estimation methods applied to fissure and karst aquifers of the Lagoa Santa Karst Environmental Protection Area, Brazil, Hydrological Processes, 37, e14 971, 2023.

Warren, J. E. and Root, P. J.: The Behavior of Naturally Fractured Reservoirs, SPE Journal, 3, 245–255, https://doi.org/10.2118/426-PA, 1963.

Whitaker, S.: The Forchheimer equation: A theoretical development, Transport in Porous Media, 25, 27–61, https://doi.org/10.1007/BF00141261, 1996.

Wittenberg, H.: Baseflow recession and recharge as nonlinear storage processes, Hydrological Processes, 13, 715–726, 1999.

https://doi.org/10.5194/egusphere-2025-6044
Preprint. Discussion started: 3 February 2026

Xu, B., Ye, M., Dong, S., et al.: A new model for simulating spring discharge recession and estimating effective porosity of karst aquifers, Journal of Hydrology, 562, 609–622, 2018.

Zhang, R., Bu, Q., Chen, X., et al.: Can storage–discharge characteristics of karst matrix system quantified through recession analysis be reliable?, Journal of Hydrology, 648, 132 378, 2025.